Volume 396, Issue 3, 26 February 2010

ISSN 0022-2836

ELSEVIER

JMB

JOURNAL OF MOLECULAR BIOLOGY

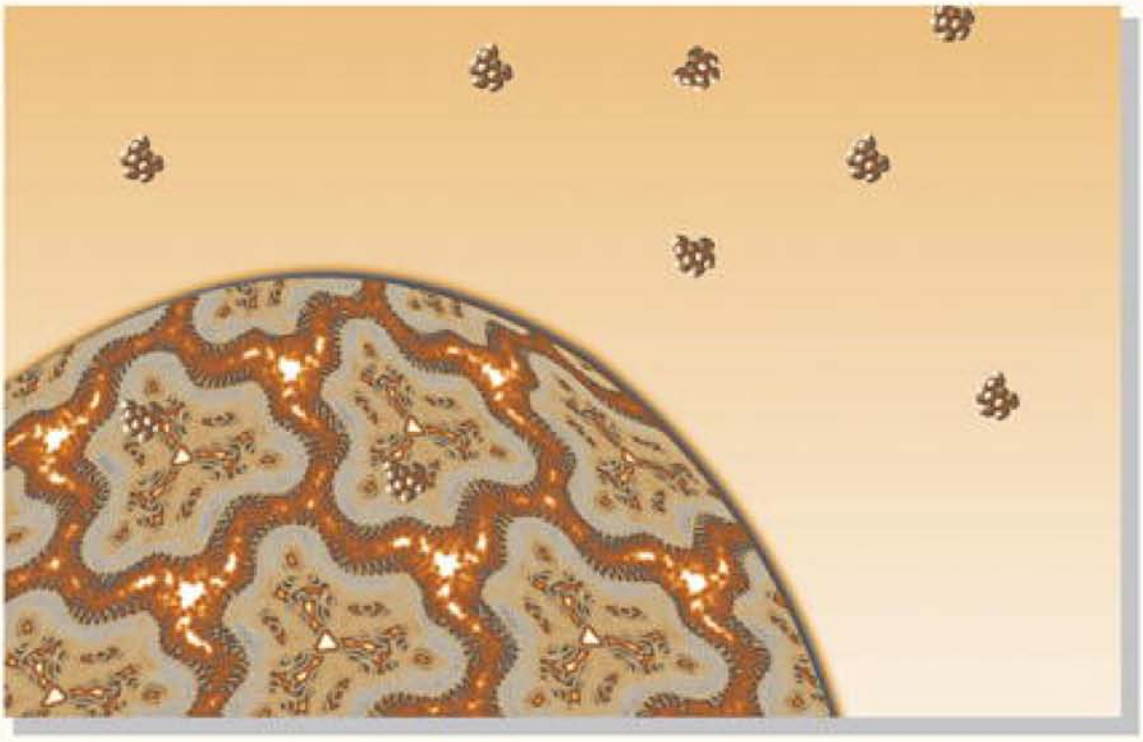

0022-2836(20100226)396:3;1-9

doi:10.1016/j.jmb.2009.12.010 J. Mol. Biol. (2010) 396, 593–601

JMB

Available online at www.sciencedirect.com

ScienceDirect

ELSEVIER

The Prototypical H+/Galactose Symporter GalP Assembles into Functional Trimers

Hongjin Zheng[1], Justin Taraska[2,3], Alexey J. Merz[1] and Tamir Gonen[1,3]*

[1]*Department of Biochemistry, University of Washington, 1705 NE Pacific Street, Seattle, WA 98195, USA*

[2]*Physiology and Biophysics, University of Washington, 1705 NE Pacific Street, Seattle, WA 98195, USA*

[3]*Howard Hughes Medical Institute*

Received 19 August 2009; received in revised form 30 November 2009; accepted 8 December 2009
Available online 16 December 2009

Edited by W. Baumeister

Glucose is a primary source of energy for human cells. Glucose transporters form specialized membrane channels for the transport of sugars into and out of cells. Galactose permease (GalP) is the closest bacterial homolog of human facilitated glucose transporters. Here, we report the functional reconstitution and 2D crystallization of GalP. Single particle electron microscopy analysis of purified GalP shows that the protein assembles as an oligomer with three distinct densities. Reconstitution assays yield 2D GalP crystals that exhibit a hexagonal array having p3 symmetry. The projection structure of GalP at 18 Å resolution shows that the protein is trimeric. Each monomer in the trimer forms its own channel, but an additional cavity (10~15 Å in diameter) is apparent at the 3-fold axis of the oligomer. We show that the crystalline GalP is able to selectively bind substrate, suggesting that the trimeric form is biologically active.

Keywords: two-dimensional crystals (2D crystals); electron crystallography; galactose permease (GalP); H^+/galactose symport; glucose transporter (GLUT)

Introduction

The primary source of energy for human cells is glucose. Glucose is transported from the intestines into the blood stream and finally into various cell types through glucose transporters, which are proteins that form specialized gateways for the transport of sugars across biological membranes.[1] At least two different transport mechanisms exist for the uptake of glucose in mammalian cells. The first is through the facilitative glucose transporters (GLUTs)[2] and the second is through the sodium-coupled glucose transporters.[3] Bacteria also express a third type of sugar transporter, the proton-coupled glucose transporter.[4,5]

Glucose transporters are members of the major facilitator superfamily (MFS), which includes >15,000 identified membrane proteins[6] that transport diverse substrates such as ions, drugs, nucleosides, amino acids, neurotransmitters, peptides, and sugars (for a review see Ref. 7). To date, high-resolution structures for three members of the MFS have been determined,[8–10] showing a conserved overall architecture. MFS proteins fold into 12 transmembrane α helices with the N- and C-termini localized cytoplasmically.[7] Structurally, every MFS member studied to date is divided into halves, each comprising a bundle of six transmembrane α-helical domains. The two halves are connected by a long hydrophilic cytoplasmic loop between transmembrane helices 6 and 7.[6] In all structures studied, the channel or pore is formed at the interface of the two halves of the protein.[8–10]

Every tissue in the human body expresses one or more types of the facilitated glucose transporter (GLUT) isoforms. Thus far 14 isoforms have been identified in humans (GLUT1–GLUT14).[11] Each GLUT isoform has different substrate affinities and transport properties. For example, GLUT1 transports glucose and galactose highly efficiently but is only leaky to fructose. In contrast, GLUT5 transports fructose highly efficiently and is only leaky to glucose and galactose.[12] The expression of different

**Corresponding author.* Department of Biochemistry, University of Washington, 1705 NE Pacific Street, Seattle, WA 98195, USA. E-mail address: tgonen@u.washington.edu.

Abbreviations used: GLUT, glucose transporter; GalP, galactose permease; DM, n-decyl-β-d-maltopyranoside; DMPC, 1,2-dimyristoyl-sn-glycero-3-phosphocholine.

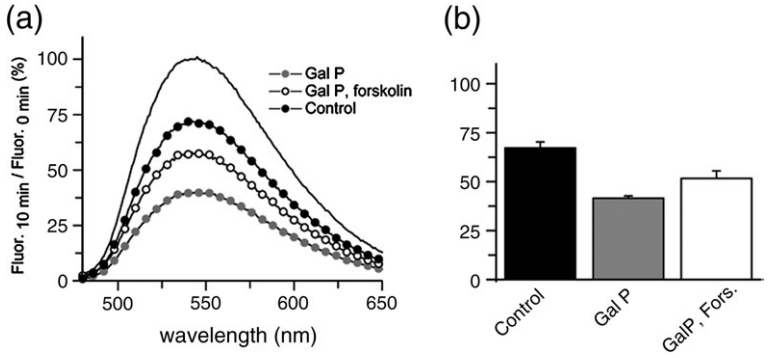

Fig. 1. Glucose uptake studies in bacterial cells show that recombinant GalP is active. (a) Spectra of cultures transformed with GalP (gray symbols) or control vector (black symbols) after 10 min incubation in the presence of the fluorescent glucose analog 2-NBDG.[28] Cultures transformed with GalP in the presence of the inhibitor forskolin are shown as open symbols.[26] The initial fluorescence of the cultures is shown as a black line. The loss of fluorescence was measured as the bacteria transported the fluorescent glucose into the cells and broke down the sugar into a non-fluorescent form.[29] Medium containing GalP-expressing bacteria (gray symbols) showed a rapid decrease in fluorescence when compared with control cells (black symbols). (b) Average decrease in 2-NBDG fluorescence in cells transformed with GalP, GalP in the presence of forskolin, or control plasmid at 10 min. Error bars represent the s.e.m ($n = 5$).

GLUT isoforms in different tissues reflects the specific needs of individual tissues. Not surprisingly, malfunctions or mutations in GLUT isoforms result in diverse medical conditions and diseases. GLUT1 deficiency syndrome results in impaired glucose uptake across the blood–brain barrier.[1,13–15] Similarly, impaired glucose uptake through GLUT4 is linked to diabetes, a disease reaching epidemic proportions in industrialized nations.[16–19] Moreover, most known cancers over-express various GLUT isoforms, supplying the nutrients needed to support uncontrolled cell proliferation.[20]

The closest *Escherichia coli* homolog to the human GLUT1 is galactose permease (GalP).[21–23] GalP couples the transport of a proton to the transport of a monosaccharide and is therefore a H^+/monosaccharide symporter. Notably, in the absence of a proton gradient,GalP still transports glucose, but at a much lower rate.[24,25] In this way, GalP closely resembles the facilitated GLUTs in humans. Moreover, GalP and human GLUT1 share 29% identity and indeed both transporters have similar sugar specificity, high affinity for glucose and galactose, but much lower affinity for fructose.[12] Both transporters are inhibited by cytochalasin B and forskolin.[26,27]

We report the expression, purification and 2D crystallization of the bacterial H^+/galactose symporter GalP. We find that purified GalP forms oligomers, as indicated by size-exclusion chromatography and single particle averaging. The projection structure of GalP, determined by electron crystallography of 2D crystals, indicates that the protein forms trimers in the lipid bilayer. We show that the 2D crystals contain GalP trimers that are able to bind substrate, suggesting that trimerization is biologically relevant.

Results

Recombinant GalP that is targeted to bacterial membranes is active

We cloned full-length GalP from *E. coli* genomic DNA and overproduced it as a His_6-tagged fusion protein in *E. coli* cells. Although membrane protein production can be straightforward, quite often some of the overproduced protein is not folded properly, is not inserted into the membranes and is non-functional. Assuming that the protein is inserted into the membrane of the host cells, it is likely that it is also folded properly and therefore should show activity. We therefore subjected the GalP-expressing cells to glucose uptake studies to assay whether the GalP that is incorporated into the bacterial cell membrane showed any activity; in other words, could the recombinant GalP transport glucose? The GalP-overproducing cells were sedimented and resuspended in sugar-free buffer at pH 7.2 and starved for 1 h. The bacteria were then transferred to a pH 6.5 buffer containing the fluorescent glucose analog 2-NBDG.[28] The change in pH established the H^+ gradient needed to activate GalP. The loss of fluorescence was measured as the bacteria transported the fluorescent glucose into the cells and broke down the sugar into a non-fluorescent form.[29] Medium containing GalP-expressing bacteria showed a rapid decrease in fluorescence when compared with control cells (Fig. 1). Glucose uptake was largely inhibited by the addition of forskolin. These results show that the GalP is active and that the N-terminal His_6 tag does not interfere with the transporter's structure or function.

The glucose uptake results indicated that the GalP that is inserted into the bacterial membrane is active and, therefore, represents a good candidate for structure studies. We used differential centrifugation and incubation with chaotropic agents to isolate the membrane fraction and discard all the GalP that did not insert into the bacterial membrane. GalP-expressing bacteria were broken in a microfluidizer and crude membrane extracts prepared as described in Materials and Methods. Crude membrane extracts were subjected to stripping with 4 M urea followed by treatment with 20 mM NaOH to remove any protein that was not incorporated into the cell membrane.[30] More than 50% of the recombinant GalP was removed by these stringent stripping conditions, as judged by SDS-PAGE (data

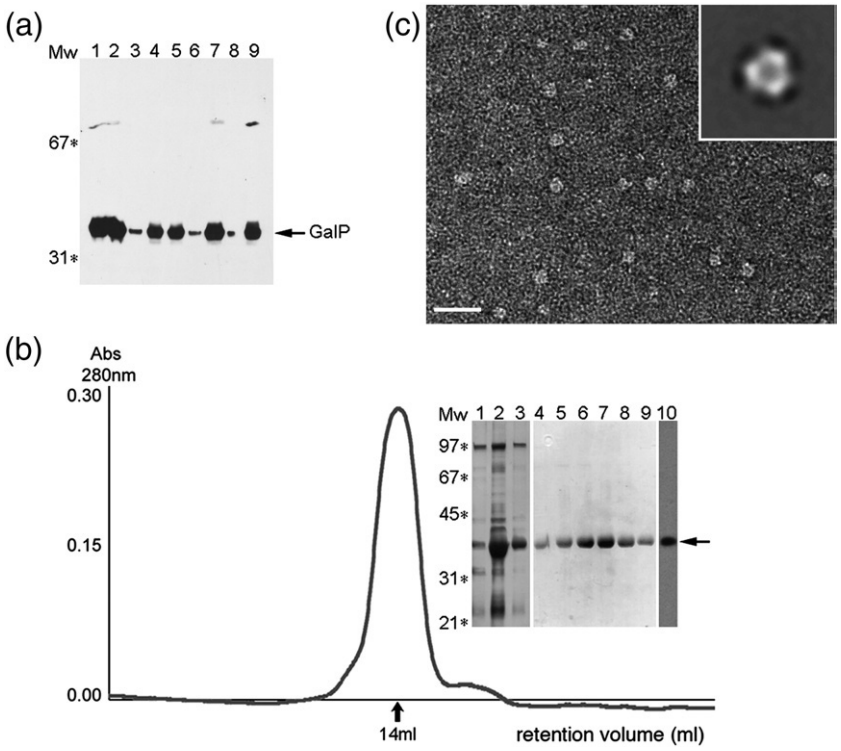

Fig. 2. Recombinant GalP is an oligomer. (a) Western blot analysis of GalP solubilization assays. Molecular mass markers as indicated in kDa. Lane 1, starting material (bacterial cell membranes). Lanes 2 and 3, DM soluble and insoluble fractions, respectively. Lanes 4 and 5, n-dodecyl-β-d-maltopyranoside soluble and insoluble fractions, respectively. Lanes 6 and 7, OG soluble and insoluble fractions, respectively. Lanes 8 and 9, Chaps soluble and insoluble fractions, respectively. DM is the only detergent able to solubilize large quantities of GalP. (b) His_6-tagged GalP was purified using a combination of Ni^{2+}-NTA and size-exclusion chromatography. The chromatogram for the size-exclusion column is shown. The transporter eluted from the gel-filtration column at 14 ml corresponding to a molecular mass of ~220 kDa. This size is most consistent with a GalP trimer. Inset, SDS PAGE documentation of the GalP purification process. Molecular mass markers are indicated in kDa. Lanes 1-3, Ni-NTA column fractions (load, wash with 50 mM imidazole and elute with 300 mM imidazole, respectively). The elution shown in lane 3 was used for subsequent gel-filtration experiments. Lanes 4–9, gel-filtration column fractions from the elution profile presented in (b). GalP from lane 7 was used for the subsequent electron microscopy analysis presented in (c). Lane 10, Western blot analysis identifying His_6-tagged GalP (Pierce His-probe). (c) Purified GalP was negatively stained with uranyl formate and imaged in a transmission electron microscope. The scale bar represents 20 nm. Inset: A calculated projection average of GalP. The length of the side of the box is 170 Å. The particle appears triangular with three distinct densities. The calculated mass of this particle is consistent with a GalP trimer.

not shown). Therefore, although milligram amounts of GalP were manufactured per liter of cells, a large fraction of the GalP did not insert into the bacterial cell membrane and was therefore discarded. The remaining GalP survived the stripping because it was embedded in, and protected by, the bacterial lipid bilayer.

GalP is an oligomer

The studies discussed above indicated that recombinant GalP is functional and is therefore folded correctly and suitable for structural analysis. We proceeded with large-scale production of the protein and purification en route to 2D crystallization and structural analysis. Expression levels of GalP were examined by Western blotting and high-level expressing clones were used for large-scale production of the protein. Treatment of GalP-expressing cells with a microfluidizer (Emulsiflex) at 15,000 psi (1 psi ≈ 6.9 Pa) effectively ruptured all membranes and allowed us to harvest membrane pellets following extensive washing by centrifugation and incubation with chaotropic agents as described above. These membranes were stored at −20 °C.

More than 90% of GalP was solubilized in the presence of 1% (w/v) n-decyl-β-d-maltopyranoside (DM). GalP appeared as a single band on SDS-PAGE with an apparent molecular mass of 36 kDa (Fig. 2). Western blotting analysis as well as mass spectrometry confirmed that the ~36 kDa band is indeed GalP (data not shown) in good agreement with earlier reports.[26] We followed the solubilization of His_6-tagged GalP by Western blotting using a His probe (Pierce) (Fig. 2a). Four different detergents were assayed: DM, n-octyl-β-D-glucopyranoside, n-dodecyl-β-D-maltopyranoside and Chaps, and the solubilization efficiency analyzed by SDS-PAGE and Western blotting. The best results were obtained with DM (Fig. 2a lane 2 *versus* 3).

GalP was purified using a combination of Ni^{2+}-NTA and size-exclusion chromatography (Fig. 2b). Following solubilization with DM, His_6-tagged GalP was incubated with Ni^{2+}-NTA resin at 4 °C for 2 h. The resin was loaded into a drip column, washed with 50 mM imidazole to remove any non-specific binders, and GalP was eluted with 300 mM imidazole (Fig. 2b, gel lanes 1–3). Following purification on Ni^{2+}-NTA, GalP was further purified on a Superdex 200 size–exclusion chromatography column (Pharmacia). GalP eluted as a single symmetric peak with a retention volume of 14 ml (Fig. 2b, gel lanes 4–9). This retention volume corresponds to a molecular mass of ~220 kDa. Since the calculated molecular mass of GalP is ~50 kDa and we expect the mass of the detergent micelle to be ~35 kDa (as

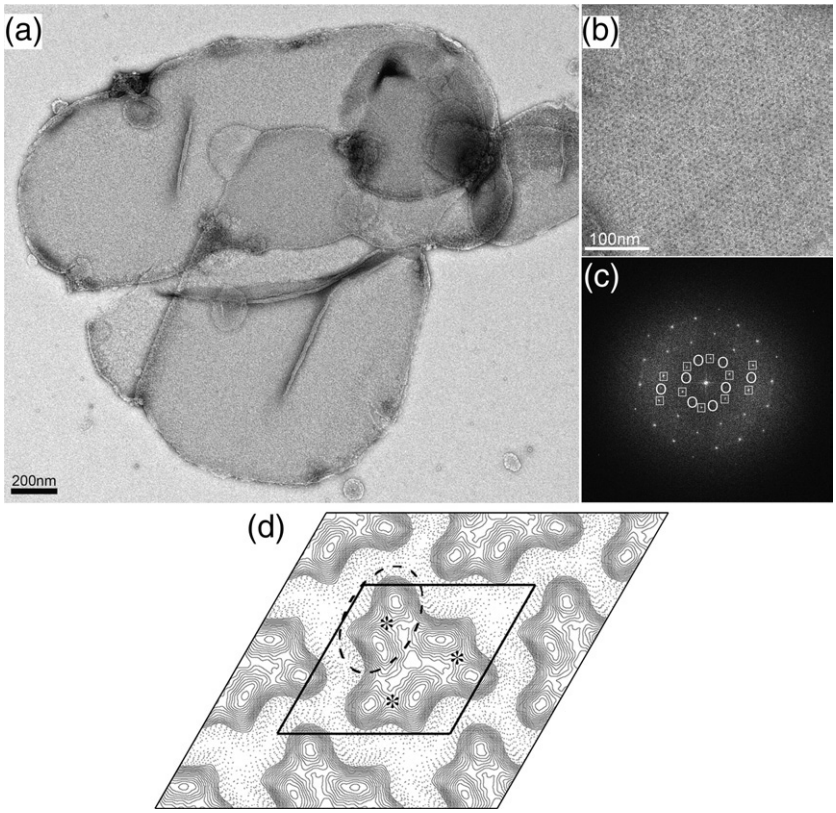

Fig. 3. Two-dimensional crystallization and projection structure of trimeric GalP. (a) Reconstitution experiments of purified GalP with DMPC yield large and well-ordered 2D crystals. These crystalline vesicles are ~2 μm in diameter. (b) A close-up view of negatively stained GalP 2D crystals exhibits a hexagonal array. (c) Fourier transform of the image in (b) showing strong and sharp diffraction spots. Two sets of diffraction spots are indicated by squares and circles. (d) Projection map of negatively stained GalP 2D crystals with imposed p3 symmetry at 18 Å resolution. The hexagonal unit cell dimensions are $a=b=75$ Å and $\gamma=120°$. The black outline indicates a unit cell. The broken-line circle indicates a GalP monomer in the trimeric assembly. Each monomer appears to contain two densities, probably representing the two pseudo-symmetric halves of GalP. Each GalP monomer contains its own channel. The asterisk denotes the postulated location of the transporter's channel based on other MFS structures.[8–10]

was the case with the lens membrane protein MP20[31]), the ~220 kDa peak most likely corresponds to a GalP trimer or a tetramer.

Single particle analysis of purified GalP indicated that the protein is an oligomer with an overall 3-fold rotational symmetry. Shortly after purification using size-exclusion chromatography (see above), recombinant GalP was negatively stained with uranyl formate as described,[32] and viewed in an electron microscope. A representative electron micrograph of the preparation is presented in Fig. 2c. GalP particles appeared homogeneous in size and no aggregation was observed. A total of 8723 individual particles were selected in WEB and processed in SPIDER using established protocols to classify the particles and calculate projection averages.[33] An example of a GalP projection average is presented in Fig. 2c (inset). In projection averages, GalP appeared as a triangular particle with an apparent cavity at its center. Assuming the height of the particle vertical to the projection plane is ~60 Å and a protein density of 0.81 Da/Å^3, densities in the projection average would accommodate a protein mass of ~140 kDa in total and is in agreement with GalP trimers.

Electron crystallography of GalP

The 2D crystallization of GalP shows that the protein is a trimer in biological membranes. Reconstitution experiments of GalP were carried out in a range of pH values (6–10) a range of salt conditions (50–500 mM NaCl) and a range of divalent cation concentrations (0–200 mM $MgCl_2$ and/or 0–200 mM $CaCl_2$). Several lipids at various lipid to protein ratios were also assayed for reconstitution and 2D crystallization. More specifically, the lipids 1,2-dimyristoyl-sn-glycero-3-phosphocholine (DMPC), 1,2-dioleoyl-sn-glycero-3-phosphocholine, 1-palmitoyl-2-oleoyl-sn-glycero-3-phosphocholine, *E. coli* total lipid extract, heart lipid extract and liver lipid extract (Avanti Polar Lipids) were tested. The assay was performed by slow dialysis against crystallization buffer lacking the detergent as described.[34] GalP was reconstituted under all conditions tested. Well-ordered 2D crystals formed with DMPC at a lipid to protein ratio of 0.2–0.6 when dialysis was performed against a crystallization buffer containing 10 mM Tris pH 8, 150 mM NaCl and 25 mM $CaCl_2$ (Fig. 3).

GalP 2D crystals appeared vesicular with diameters of ~2 μm (Fig. 3a). Although the presence of divalent cations such as Mg^{2+} or Ca^{2+} was critical for crystal formation, the amount of either cation was apparently less important, as the 2D crystals formed using a wide range of cation concentrations without significant difference in crystal size or order. Negatively stained GalP 2D crystals appeared to contain a hexagonal lattice. The majority of the vesicles that were crystalline exhibited a lattice throughout the vesicle. Coherent crystalline regions in the vesicles were relatively large and typically were of the order of 0.5–1 μm in width (Fig. 3b). Fourier transforms showed strong and sharp spots indicating that these 2D crystals were relatively well ordered (Fig. 3c). The calculated Fourier transforms reveal two sets of diffraction spots, although one of the lattices is more complete and shows many more

Table 1. Internal phase residuals of all possible two-sided plane groups of a representative image of an untilted GalP 2D crystal

Two-sided plane group	Phase residual[a]	No. comparisons	Target residual[b]
p1	11.9[c]	56	
p2	62.3	28	17.0
p3	12.4[d]	52	11.9
p312	52.7	121	12.1
p321	26.9	127	12.4
p6	58.6	132	13.0
p622	59.1	276	12.4

Internal phase residuals were determined from spots of IQ1 – IQ4 to 18 Å resolution.
[a] Phase residual *versus* other spots (90° random).
[b] Target residual based on statistics taking Friedel weight into account.
[c] No phase comparison is possible for space group p1.
[d] Acceptable; best space group is p3.

spots (squares *versus* circles). The appearance of the two sets of diffraction spots must originate from the two layers of the collapsed vesicle, suggesting that the entire membrane area was crystalline. Images of negatively stained GalP 2D crystals were recorded on a 100 kV transmission electron microscope (Morgagni FEI) with a bottom mount 4 k×2 k CCD at a nominal magnification of 32,000×. Images were processed in MRC[35] using the 2dx interface.[36] Following CTF correction and two unbending cycles, we observed diffraction to 18 Å resolution. The GalP lattice is hexagonal with space group p3 as determined by the program ALLSPACE (Table 1).[37] The unit cell dimensions are $a=b=75$ Å and $\gamma=120°$ (Table 2). 2D crystals of this size and order ideally should be studied under cryogenic conditions without stain. A projection map of frozen-hydrated 2D crystals showing the positions of helices in the transporter could then be calculated. However, despite our very best efforts we have not been able to freeze these 2D crystals. Typically, vanishingly small numbers of the GalP 2D crystals stick to the cryo grid and the crystal packing appears to deteriorate upon freezing even when various cryo protectants were used (glucose, trehalose and various low molecular mass PEGs were all assayed at various concentrations) or when bacitracin was added.[38] As such, we are presenting the projection structure of GalP in negative stain. In projection, GalP appeared to be a trimer (Fig. 3d, monomer circled). The three GalP monomers are oriented around a single p3 rotational axis, with an apparent cavity ~10 Å in diameter at the center. Each monomer consists of two distinct densities, most likely belonging to the two pseudo-symmetric halves of the transporter (i.e., 2×6 α-helices common to MFS members). As with other MFS members,[8–10] the channel in the GalP monomer is probably formed at the interface between these two pseudo-symmetric regions (Fig. 3d, asterisk).

Crystal packing in GalP 2D crystals appears to be mediated by lipids. Protein–protein interactions are often crucial in the formation of 3D crystals used for X-ray crystallography. In electron crystallography, however, it appears that lipids also play an important role in mediating crystal packing. Indeed, both the type of lipid used and the lipid to protein ratio used are major parameters assayed during the 2D crystallization process.[34] For example, lipids mediated crystal contacts in both aquaporin-0[39] and bacteriorhodopsin[40–42] 2D crytals. In both cases, neighboring protein molecules were separated laterally from one another by 10~15 Å; and this space was filled with an annular shell of the lipid bilayer that mediated the crystal contacts.[43] Similarly, neighboring GalP molecules are separated laterally from one another by 10~15 Å (Fig. 3d), suggesting that lipids may mediate crystal contacts in these 2D crystals as well. It is unclear at this stage what kind of specific lipid–protein interactions are involved. Nor is it clear if only annular lipids are involved (lipids bound directly to the protein) or if bulk lipids also play a role (lipids interacting with other lipids but having no direct contact with the protein).

Crystalline GalP can bind substrate

Subsequent functional studies show that the GalP 2D crystals contain a transporter that is able to bind substrate. Because the GalP 2D crystals are vesicular, we used fluorescence microscopy to investigate transporter function by measuring binding (or uptake) of the fluorescent glucose analog 2-NBDG.[28] GalP is highly permeable to glucose, but not to lactose.[44] Even in the absence of a proton gradient, GalP is able to transport glucose but ~100× less efficiently.[12] To assay the association of GalP with 2-NBDG, GalP 2D crystals grown at pH 8 were pre-incubated at pH 7.5 at room temperature for 1 h in the presence of 2 mM glucose (to compete with 2-NBDG) or 2 mM lactose (which should not compete with 2-NBDG). The 2-NBDG was then added to the vesicles (2 μM, pH 7.5) and incubated overnight at 4 °C. The resulting preparations were imaged using a wide-field fluorescent microscope equipped with an EMCCD camera (Fig. 4). It is important to note that the same GalP 2D crystalline vesicle preparations used for structure analysis (Fig. 3) were used for these assays. Consistent with the hypothesis that the GalP in the vesicles is active,

Table 2. Electron crystallographic data

Plane group symmetry:	p3	
No. images:	7	
Unit cell parameters:	$a=b=75$Å $\gamma=120°$	
Range of defocus (Å)	5000–15,000	
Resolution range (Å)	No. unique reflections	Phase residual (random=45)
200–47.6	3	6.6
47.5–27.4	6	14.1
27.3–21.2	9	24.1
21.1–19.4	3	27.2
19.3–18.0	8	20.5
Total range 200–18.0	29	18.5

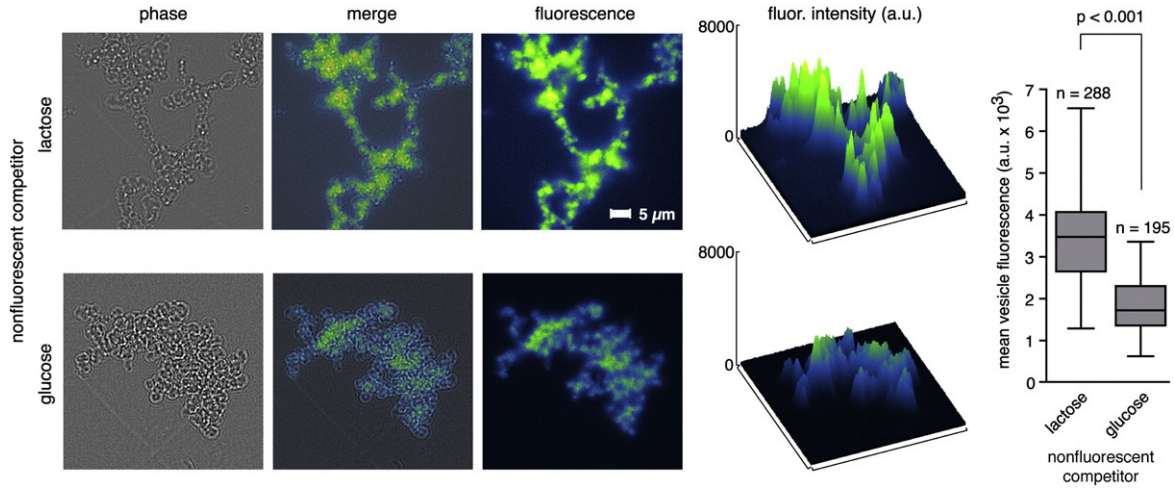

Fig. 4. GalP in 2D crystals can bind substrate. Images of vesicles pre-equilibrated with the nonfluorescent lactose (top row) or glucose (bottom row) are shown in phase contrast, fluorescence, and as merged images. Each fluorescence intensity profile is presented also as a landcape plot. On the right, box plots show summary statistics for intensity measurement of hundreds of individual vesicles. Boxes indicate mean and interquartile range, and whiskers indicate 1.5 × the interquartile range. The significance value shown is from a Mann-Whitney *U*-test comparing the two treatment groups. The sample pre-equilibrated with lactose accumulated significantly more of the fluorescent 2-NBDG than the sample with pre-equilibrated with glucose, indicating that the GalP transporter is active and is selective for glucose and excludes lactose. It is important to note that the same GalP 2D crystalline vesicle preparations used for structure analysis was used for these function assays.

we found that vesicles pre-incubated in the presence of lactose exhibited much more 2-NBDG fluorescence than vesicles pre-incubated with glucose (Fig. 4, right-hand panel, $p<0.001$, Mann-Whitney *U*-test). This is because glucose is a competitor for 2-NBDG binding to GalP but lactose is not.[12] Thus, GalP trimers embedded within 2D crystals bind substrate and are selective for glucose in preference to lactose. It is possible that our GalP 2D crystals contain a small fraction of non-crystalline GalP, and with this assay it is impossible to distinguish between 2-NBDG binding to crystalline or to non-crystalline GalP. The fluorescence experiments lack the spatial resolution needed to distinguish between the two. We further note that we cannot distinguish unambiguously between substrate binding and active transport. It is possible that GalP is binding glucose but not transporting it into the vesicles. In further control experiments, protein-free vesicles also bound some 2-NBDG, but in contrast to the GalP 2D crystals, this binding was not affected by the presence of glucose or lactose, indicating that 2-NBDG binding to protein-free vesicles is nonspecific (data not shown).

Discussion

Our studies show that the H^+/galactose symporter from *E. coli*, GalP, forms trimers that are able to selectively bind substrate. GalP is the closest bacterial homolog to the facilitative human glucose transporters, members of which are involved in diverse medical conditions ranging from diabetes to cancer and epilepsy.[17,18,20,45] Reconstitution and 2D crystallization of recombinant GalP yielded well ordered hexagonal crystalline vesicles that contain trimeric GalP as its building block. We show that the GalP trimers are able to bind substrate and therefore likely represent the biologically active species.

GalP appears to be the first MFS member shown to assemble into trimers. Although more then 15,000 members of the MFS have been identified,[6] the high-resolution crystal structures of only three members are known: the lactose permease LacY; the glycerol 3-phosphate transporter GlpT; and the multidrug transporter EmrD.[8–10] In addition, the 6 Å resolution structure of the bacterial oxalate transporter OxlT was determined by electron crystallography.[46] In all four cases, the transporters appeared as monomers, although a number of monomers occupied the unit cell and formed crystallographic contacts.[8–10,47–50]

GalP is trimeric both in solution as a detergent-solubilized protein and when it is embedded in the lipid bilayer. It is possible that trimerization is needed for the structural stability of GalP. For example, aquaporins and bacteriorhodopsin form oligomers, although each monomer forms its own pore.[39–41,51] In both cases, it was suggested that oligomerization is needed for the structural stability of the proteins. As with other MFS members,[8–10] it is likely that each GalP monomer forms its own pore (Fig. 3d, asterisk) and it might be that the GalP trimer is simply a structurally stable assembly.

Another possibility is that GalP trimerization is important for transporter function and/or regulation. Our studies show that three GalP monomers orient themselves in the oligomer around a single p3 rotational axis. A rotational axis of various symmetries is often observed in structures of membrane proteins. There is increasing evidence that the oligomerization is important for the function of

some of these proteins, because regulatory ligands and substrates often localize either to the subunit interface or bind within the axial cavity along the symmetry axis.[52] Similarly, it is possible that trimerization of GalP could have implications for co-operativity in the transport mechanism and/or the regulation of the transporter by ligands. Trimerization could also be important for the binding of regulatory proteins to the GalP as in the case of aquaporin-0 regulation by Ca^{2+}/calmodulin.[53]

The cavity formed at the symmetry axis of some membrane proteins is filled with lipid molecules. Bacteriorhodopsin forms trimers and the cavity at its 3-fold axis is filled with lipid molecules that are required for protein function.[40,42,54] In sharp contrast, GalP has no known functional requirement for lipids and, in fact, in our assays GalP is active both in bacterial cells (i.e., embedded in *E. coli* native lipids; Fig. 1) and in 2D crystals formed with the synthetic lipid DMPC (Fig. 4). While we cannot exclude the possibility that the 3-fold axis of the GalP trimer is also filled with lipid molecules (as with bacteriorhodopsin[40,42,54]), we also cannot exclude the possibility that: (I) allostery plays a critical role in the function and/or regulation of GalP; or (II) that the 3-fold axis of GalP is open, and forms an additional (or new) channel yet to be structurally and functionally characterized. An atomic-resolution structure of GalP determined in the context of the lipid bilayer is required before answers to these fundamental questions can be found.

Materials and Methods

Protein expression and purification

Full-length galactose permease was cloned from *E. coli* genomic DNA into the expression vector pET15b with an N-terminal His_6 tag, and expressed in *E. coli* BL21 Star cells (Invitrogen). Cells were harvested after expression overnight at 37 °C and subjected to three cycles of disruption in a micro-fluidizer at 15,000 psi. The suspension was centrifuged at 15,000*g* for 30 min to remove large cell debris, and then centrifuged at 130,000*g* for 1 h to collect a membrane-enriched pellet. The pellet was typically washed with 4 M urea and 20 mM NaOH and re-sedimented at 130,000*g* before suspending it in 20 mM Tris–HCl (pH 8) buffer for storage at −20 °C.

The solubilization assay was done as follows. Four different detergents were assayed: 1% DM, 5% (w/v) n-octyl-β-d-glucopyranoside. 0.5% (w/v) n-dodecyl-β-d-maltopyranoside (DDM) and 5% (w/v) Chaps. Each reaction tube contained 100 μl of washed membranes (prepared as described above) into which an equal volume of the detergent was added in 10 mM Tris buffer pH 8.0. The mixture was then incubated at 4 °C, or at room temperature or at 37 °C for 15, 30 or 60 min. Soluble material was separated from insoluble material by ultracentrifugation at 160,000*g* using a Beckman Optima and the samples were analyzed by SDS-PAGE and Western blotting. No significant difference was observed among the different temperatures or lengths of incubation with detergent. Typically, DM gave the best results. Fig. 2a shows the solubilization assay for 60 min at 4 °C.

Membranes were solubilized with 1% (w/v) DM at 4 °C in 20 mM Tris-HCl (pH 8), 150 mM NaCl for 45 min. After centrifugation at 160,000*g* for 30 min, the supernatant was loaded onto a Ni^{2+}-NTA column. Bound material was washed with buffer containing 50 mM imidazole and eluted with 300 mM imidazole. Eluted GalP was subjected to size-exclusion chromatography on a Superdex 200 column pre-equilibrated with 20 mM Tris–HCl pH 8, 150 mM NaCl and 0.3% DM. For size measurements, the Superdex 200 column was calibrated using ovalbumin, bovine serum albumin (BSA), aldolase, chymotrypsinogen A, and ribonuclease A standards, and blue dextran was used for determination of the void column volume. For the calculation of molecular size, a calibration plot of log M_w *versus* K_{av} was constructed:

$$K_{av}=(V_c-V_0/V_t-V_0)$$

where V_c is the protein elution volume, V_t is the column volume (24 ml) and V_0 is the void column volume. The retention volume for GalP was 14 ml, corresponding to a molecular size of ~220 kDa.

Single particle electron microscopy of detergent-solubilized GalP

Purified GalP in DM solution was stained by 0.75% (w/v) uranyl formate as described.[32] Single particle data were collected in a transmission electron microscope (Morgagni M268, FEI, Hillsboro, OR) equipped with a tungsten filament and operating at an acceleration voltage of 100 kV. All images were recorded at a magnification of 67,000× on 4 k×2 k Gatan CCD corresponding to a final pixel size of 1.34 Å on the specimen level. In all, 8723 particles were selected and windowed into 128×128 pixel images using WEB.[33] Projection averages were generated after eight cycles of reference-free multivariate statistical analysis in SPIDER using established procedures.[33] Symmetry was applied in EMAN.[55] For size calculations, the GalP projection average was treated as an irregular shape with an assumed thickness of 60 Å. The entire area of the particle was fractionated into a series of triangles and rectangles, and a volume for each triangle and rectangle was calculated. The calculated volumes were then summed and multiplied by 0.81 Da/Å^3. Finally, the area of the apparent pore in the center of the particle was subtracted.

Two-dimensional crystallization and image processing

Purified protein at a concentration of either 0.5 mg/ml or 1 mg/ml was mixed with DMPC lipids (Sigma) at lipid to protein ratios of 0.2–0.6 (w/w). The mixtures were dialyzed against 10 mM Tris–HCl (pH 8), 150 mM NaCl, 25 mM $CaCl_2$, 0.02% (w/v) NaN_3 at room temperature. Following dialysis, the crystallization buttons were opened; samples were negatively stained with 0.75% uranyl formate as described[56] and viewed in a transmission electron microscope operating at 100 kV (Morgagni M268, FEI, Hillsboro, OR). Images of GalP 2D crystals were recorded on a 4 k×2 k Gatan CCD at a magnification of 32,000× resulting with a pixel size of 2.8 Å at the specimen level. Images of well diffracting 2D crystals were processed in the MRC suite of programs[35] through the 2dx interface,[36,57] using well-established protocols.[42]

Glucose uptake and binding studies

For glucose uptake studies in bacteria, BL21 Star cells (Invitrogen) were transformed with the GalP-pET15b plasmid (or pET15b as a control) and grown overnight in

Luria broth. Cells were pelleted and resuspended in M9 minimal medium without sugars (pH 7.2) and starved for 1 h at 37 °C. The cells were then pelleted and resuspended to a final concentration of 1.4 $A_{600\ nm}$ in acidic bacterial buffer containing 150 mM NaCl, 5 mM Hepes pH 6.5. Glucose uptake was measured by adding glycerol to a final concentration of 10 mM, and the fluorescent glucose analog 2-NBDG[28] to a final concentration of 10 μM. The loss of fluorescence from the solution was monitored with a Fluorolog-3 fluorimeter (Horiba Jobin Yvon). As a control, cells not expressing GalP were used and treated as above. For inhibition, 30 μM forskolin was added to the experiments.[26]

For binding studies using GalP 2D crystals, vesicles containing crystalline GalP at pH 8 were incubated at room temperature for 1 h with 2 mM lactose at pH 7.5. The sample was then incubated overnight at 4 °C with 2 μM 2-NBDG.[28] A 5 μl drop of the preparation was applied onto a glass slide, covered with a coverslip and viewed using an Olympus IX17 fluorescence microscope equipped with either a 100×, 1.3 NA or 60×, 1.45 NA objective, an EMCCD camera (Andor), and GFP filters (Semrock). Control experiments were identical, except that vesicles were incubated with 2 mM glucose instead of lactose. Circular regions (400 nm diameter) of interest, corresponding to individual vesicles, were identified and the mean fluorescence of each region was measured. The distributions of the mean vesicle fluorescence measurements were analyzed using the Mann-Whitney *U*-test. These experiments were done twice, yielding similar results. As further controls, protein-free vesicles were treated as described above either with glucose or lactose. Protein-free vesicles were prepared by slow dialysis of 20 μg of detergent solubilized DMPC against 1 l of 20 mM Mes pH 6, 50 mM $MgCl_2$ and 150 mM NaCl.

Acknowledgements

We thank the Murdock Charitable Trust and the Washington Research Foundation for generous support of our electron cryomicroscopy facility. Research in the Gonen laboratory is supported by the American Diabetes Association Award # 1-09-CD-05 and by the National Institutes of Health GM079233. Membrane biology research in the Merz laboratory is supported by the National Institutes of Health GM077349. T.G. is a Howard Hughes Medical Institute Early Career Scientist. The authors declare that none has a financial interest related to this work.

References

1. Maher, F., Vannucci, S. J. & Simpson, I. A. (1994). Glucose transporter proteins in brain. *FASEB J.* **8**, 1003–1011.
2. Hediger, M. A. (1994). Structure, function and evolution of solute transporters in prokaryotes and eukaryotes. *J. Exp. Biol.* **196**, 15–49.
3. Crane, R. K. (1960). Intestinal absorption of sugars. *Physiol. Rev.* **40**, 789–825.
4. Bissett, D. L. & Anderson, R. L. (1974). Lactose and D-galactose metabolism in group N streptococci: presence of enzymes for both the D-galactose 1-phosphate and D-tagatose 6-phosphate pathways. *J. Bacteriol.* **117**, 318–320.
5. LeBlanc, D. J., Crow, V. L., Lee, L. N. & Garon, C. F. (1979). Influence of the lactose plasmid on the metabolism of galactose by Streptococcus lactis. *J. Bacteriol.* **137**, 878–884.
6. Law, C. J., Maloney, P. C. & Wang, D. N. (2008). Ins and outs of major facilitator superfamily antiporters. *Annu. Rev. Microbiol.* **62**, 289–305.
7. Saier, M. H., Jr, Beatty, J. T., Goffeau, A., Harley, K. T., Heijne, W. H., Huang, S. C. *et al.* (1999). The major facilitator superfamily. *J. Mol. Microbiol. Biotechnol.* **1**, 257–279.
8. Abramson, J., Smirnova, I., Kasho, V., Verner, G., Iwata, S. & Kaback, H. R. (2003). The lactose permease of Escherichia coli: overall structure, the sugar-binding site and the alternating access model for transport. *FEBS Lett.* **555**, 96–101.
9. Huang, Y., Lemieux, M. J., Song, J., Auer, M. & Wang, D. N. (2003). Structure and mechanism of the glycerol-3-phosphate transporter from Escherichia coli. *Science*, **301**, 616–620.
10. Yin, Y., He, X., Szewczyk, P., Nguyen, T. & Chang, G. (2006). Structure of the multidrug transporter EmrD from Escherichia coli. *Science*, **312**, 741–744.
11. Wu, X. & Freeze, H. H. (2002). GLUT14, a duplicon of GLUT3, is specifically expressed in testis as alternative splice forms. *Genomics*, **80**, 553–557.
12. Walmsley, A. R., Barrett, M. P., Bringaud, F. & Gould, G. W. (1998). Sugar transporters from bacteria, parasites and mammals: structure-activity relationships. *Trends Biochem. Sci.* **23**, 476–481.
13. De Vivo, D. C., Leary, L. & Wang, D. (2002). Glucose transporter 1 deficiency syndrome and other glycolytic defects. *J. Child. Neurol.* **17**, 3S15–25.
14. Pascual, J. M., Lecumberri, B., Wang, D., Yang, R., Engelstad, K. & De Vivo, D. C. (2004). Type 1 glucose transporter (Glut1) deficiency: manifestations of a hereditary neurological syndrome. *Rev. Neurol.* **38**, 860–864.
15. Pascual, J. M., Wang, D., Lecumberri, B., Yang, H., Mao, X., Yang, R. & De Vivo, D. C. (2004). GLUT1 deficiency and other glucose transporter diseases. *Eur. J. Endocrinol.* **150**, 627–633.
16. Shepherd, P. R. & Kahn, B. B. (1999). Glucose transporters and insulin action-implications for insulin resistance and diabetes mellitus. *N. Engl. J. Med.* **341**, 248–257.
17. Jung, C. Y. & Lee, W. (1999). Glucose transporters and insulin action: some insights into diabetes management. *Arch. Pharm. Res.* **22**, 329–334.
18. Paternostro, G., Pagano, D., Gnecchi-Ruscone, T., Bonser, R. S. & Camici, P. G. (1999). Insulin resistance in patients with cardiac hypertrophy. *Cardiovasc. Res.* **42**, 246–253.
19. Huang, S. & Czech, M. P. (2007). The GLUT4 glucose transporter. *Cell Metab.* **5**, 237–252.
20. Medina, R. A. & Owen, G. I. (2002). Glucose transporters: expression, regulation and cancer. *Biol. Res.* **35**, 9–26.
21. Baldwin, S. A. & Henderson, P. J. (1989). Homologies between sugar transporters from eukaryotes and prokaryotes. *Annu. Rev. Physiol.* **51**, 459–471.
22. Barnett, J. E., Holman, G. D. & Munday, K. A. (1973). Structural requirements for binding to the sugar-transport system of the human erythrocyte. *Biochem. J.* **131**, 211–221.
23. Maiden, M. C., Davis, E. O., Baldwin, S. A., Moore, D. C. & Henderson, P. J. (1987). Mammalian and

bacterial sugar transport proteins are homologous. *Nature*, **325**, 641–643.
24. Henderson, P. J. (1993). The 12-transmembrane helix transporters. *Curr. Opin. Cell Biol.* **5**, 221–708.
25. Henderson, P. J., Roberts, P. E., Martin, G. E., Seamon, K. B., Walmsley, A. R., Rutherford, N. G. *et al.* (1993). Homologous sugar-transport proteins in microbes and man. *Biochem. Soc. Trans.* **21**, 1002–1006.
26. Martin, G. E., Seamon, K. B., Brown, F. M., Shanahan, M. F., Roberts, P. E. & Henderson, P. J. (1994). Forskolin specifically inhibits the bacterial galactose-H+ transport protein. *GalP J. Biol. Chem.* **269**, 24870–24877.
27. Walmsley, A. R., Lowe, A. G. & Henderson, P. J. (1994). The kinetics and thermodynamics of the binding of cytochalasin B to sugar transporters. *Eur. J. Biochem.* **221**, 513–522.
28. Yoshioka, K., Takahashi, H., Homma, T., Saito, M., Oh, K. B., Nemoto, Y. & Matsuoka, H. (1996). A novel fluorescent derivative of glucose applicable to the assessment of glucose uptake activity of Escherichia coli. *Biochim. Biophys. Acta*, **1289**, 5–9.
29. Yamada, K., Saito, M., Matsuoka, H. & Inagaki, N. (2007). A real-time method of imaging glucose uptake in single, living mammalian cells. *Nat. Protoc.* **2**, 753–762.
30. Gonen, T., Donaldson, P. & Kistler, J. (2000). Galectin-3 is associated with the plasma membrane of lens fiber cells. *Invest. Ophthalmol. Vis. Sci.* **41**, 199–203.
31. Gonen, T., Grey, A. C., Jacobs, M. D., Donaldson, P. J. & Kistler, J. (2001). MP20, the second most abundant lens membrane protein and member of the tetraspanin superfamily, joins the list of ligands of galectin-3. *BMC Cell. Biol.* **2**, 17.
32. Ohi, M., Li, Y., Cheng, Y. & Walz, T. (2004). Negative staining and image classification - powerful tools in modern electron microscopy. *Biol. Proc. Online*, **6**, 23–34.
33. Frank, J., Radermacher, M., Penczek, P., Zhu, J., Li, Y., Ladjadj, M. & Leith, A. (1996). SPIDER and WEB: processing and visualization of images in 3D electron microscopy and related fields. *J. Struct. Biol.* **116**, 190–199.
34. Andrews, S., Reichow, S. L. & Gonen, T. (2008). Electron crystallography of aquaporins. *IUBMB Life*, **60**, 430–436.
35. Crowther, R. A., Henderson, R. & Smith, J. M. (1996). MRC image processing programs. *J. Struct. Biol.* **116**, 9–16.
36. Gipson, B., Zeng, X., Zhang, Z. Y. & Stahlberg, H. (2007). 2dx–user-friendly image processing for 2D crystals. *J. Struct. Biol.* **157**, 64–72.
37. Valpuesta, J. M., Carrascosa, J. L. & Henderson, R. (1994). Analysis of electron microscope images and electron diffraction patterns of thin crystals of phi 29 connectors in ice. *J. Mol. Biol.* **240**, 281–287.
38. Mindell, J. A., Maduke, M., Miller, C. & Grigorieff, N. (2001). Projection structure of a ClC-type chloride channel at 6.5 Å resolution. *Nature*, **409**, 219–223.
39. Gonen, T., Cheng, Y., Sliz, P., Hiroaki, Y., Fujiyoshi, Y., Harrison, S. C. & Walz, T. (2005). Lipid-protein interactions in double-layered two-dimensional AQP0 crystals. *Nature*, **438**, 633–638.
40. Grigorieff, N., Ceska, T. A., Downing, K. H., Baldwin, J. M. & Henderson, R. (1996). Electron-crystallographic refinement of the structure of bacteriorhodopsin. *J. Mol. Biol.* **259**, 393–421.
41. Henderson, R., Baldwin, J. M., Ceska, T. A., Zemlin, F., Beckmann, E. & Downing, K. H. (1990). Model for the structure of bacteriorhodopsin based on high-resolution electron cryo-microscopy. *J. Mol. Biol.* **213**, 899–929.
42. Mitsuoka, K., Hirai, T., Murata, K., Miyazawa, A., Kidera, A., Kimura, Y. & Fujiyoshi, Y. (1999). The structure of bacteriorhodopsin at 3.0 Å resolution based on electron crystallography: implication of the charge distribution. *J. Mol. Biol.* **286**, 861–882.
43. Reichow, S. L. & Gonen, T. (2009). Lipid-protein interactions probed by electron crystallography. *Curr. Opin. Struct. Biol.* **19**, 560–565 [Epub 2009 Aug 11. Review].
44. Henderson, P. J., Baldwin, S. A., Cairns, M. T., Charalambous, B. M., Dent, H. C., Gunn, F. *et al.* (1992). Sugar-cation symport systems in bacteria. *Int. Rev. Cytol.* **137**, 149–208.
45. Douard, V. & Ferraris, R. P. (2008). Regulation of the fructose transporter GLUT5 in health and disease. *Am. J. Physiol. Endocrinol. Metab.* **295**, E227–E237.
46. Hirai, T., Heymann, J. A., Shi, D., Sarker, R., Maloney, P. C. & Subramaniam, S. (2002). Three-dimensional structure of a bacterial oxalate transporter. *Nat. Struct. Biol.* **9**, 597–600.
47. Zhuang, J., Prive, G. G., Werner, G. E., Ringler, P., Kaback, H. R. & Engel, A. (1999). Two-dimensional crystallization of Escherichia coli lactose permease. *J. Struct. Biol.* **125**, 63–75.
48. Auer, M., Kim, M. J., Lemieux, M. J., Villa, A., Song, J., Li, X. D. & Wang, D. N. (2001). High-yield expression and functional analysis of Escherichia coli glycerol-3-phosphate transporter. *Biochemistry*, **40**, 6628–6635.
49. Ambudkar, S. V., Anantharam, V. & Maloney, P. C. (1990). UhpT, the sugar phosphate antiporter of Escherichia coli, functions as a monomer. *J. Biol. Chem.* **265**, 12287–12292.
50. Heymann, J. A., Sarker, R., Hirai, T., Shi, D., Milne, J. L., Maloney, P. C. & Subramaniam, S. (2001). Projection structure and molecular architecture of OxlT, a bacterial membrane transporter. *EMBO J.* **20**, 4408–4413.
51. Gonen, T., Sliz, P., Kistler, J., Cheng, Y. & Walz, T. (2004). Aquaporin-0 membrane junctions reveal the structure of a closed water pore. *Nature*, **429**, 193–197.
52. Changeux, J. P. & Edelstein, S. J. (2005). Allosteric mechanisms of signal transduction. *Science*, **308**, 1424–1428.
53. Reichow, S. L. & Gonen, T. (2008). Noncanonical binding of calmodulin to aquaporin-0: implications for channel regulation. *Structure*, **16**, 1389–1398.
54. Wiener, M. (2006). A census of ordered lipids and detergents in X-ray crystal structures of integral membrane proteins. In *Protein–Lipid Interactions* (Tamm, L. K., ed.), pp. 95–117, WILEYVCH Verlag GmbH & Co., Weinheim.
55. Ludtke, S. J., Baldwin, P. R. & Chiu, W. (1999). EMAN: semiautomated software for high-resolution single-particle reconstructions. *J. Struct. Biol.* **128**, 82–97.
56. Gonen, T., Hite, R. K., Cheng, Y., Petre, B. M., Kistler, J. & Walz, T. (2008). Polymorphic assemblies and crystalline arrays of lens tetraspanin MP20. *J. Mol. Biol.* **376**, 380–392.
57. Gipson, B., Zeng, X. & Stahlberg, H. (2007). 2dx_merge: data management and merging for 2D crystal images. *J. Struct. Biol.* **160**, 375–384.